

Supplementary information

Short-, medium-, and long-chain chlorinated paraffins in South African indoor dust and cat hair

Martin Brits^{a,b,c}, Jacob de Boer^a, Egmont R. Rohwer^b, Jayne De Vos^c, Jana M. Weiss^d, Sicco H. Brandsma^a

^a Department of Environment and Health, Vrije Universiteit, Amsterdam, De Boelelaan 1085, 1081HV Amsterdam, The Netherlands

^b Department of Chemistry, Faculty of Natural and Agricultural Sciences, University of Pretoria, Lynnwood Road, Pretoria 0002, South Africa

^c National Metrology Institute of South Africa (NMISA), CSIR Campus, Meiring Naude Road, Pretoria 0040, South Africa

^d Department of Environmental Science and Analytical Chemistry, Stockholm University, Stockholm, SE-10691, Sweden

Table S1. Details on samples associated with vacuum cleaner bags (VD), freshly collected dust (FD) and cat hair (CH)

Table S1. Theoretical m/z ratios and isotopic abundances ratios of quantitation and qualifier $[M+Cl]^-$ ions for CPs.

Table S2. Calculated degree of chlorination for the SCCP, MCCP and LCCP technical mixtures

Table S3. Total Σ SCCPs, Σ MCCPs and Σ LCCPs concentration in $\mu\text{g/g}$ measured in the dust reference material (SRM 2585) with the degree of chlorination. Goodness-of-fit (R^2) below 0.5 are given in *italic* and highlighted red with indicated that the reported values are tentative.

Fig. S1. Composition of CPs in the dust reference material (SRM 2585) (A), Σ SCCP, Σ MCCP, and Σ LCCP composition based on carbon chain length, (B) Σ SCCP, Σ MCCP, and Σ LCCP carbon chain length in the repeat measurements, (C) Σ SCCP, Σ MCCP, and Σ LCCP composition based on chlorine substitution, (D) Σ SCCP, Σ MCCP, and Σ LCCP chlorine substitution in the repeat measurements.

Fig. S2. Non-traditional Kendrick MD plots, (A) constructed from the theoretical m/z quantitation and qualifier $[M+Cl]^-$ ions for CPs listed in Table S1, (B) constructed for VD 2, (C) and VD 6.

Fig. S3. Negative ion APCI-qTOF-MS mass scale-expanded segments of the mass spectra extracted for (A) C₁₉H₃₂Cl₈, (B) C₁₉H₃₁Cl₉, and (C) C₁₉H₃₀Cl₁₀ from (1) VD-2 and (2) VD-6.

Table S4. Total Σ SCCPs, Σ MCCPs, and Σ LCCPs concentration in $\mu\text{g/g}$ for VD, FD and CH with the degree of chlorination. The goodness of fit (R^2) below 0.5 are given in *italic* and highlighted red with indicated that the reported values are tentative.

Table S5. Comparisons of Σ SCCPs, Σ MCCPs, and Σ LCCPs concentrations ($\mu\text{g/g}$) in indoor dust.

Fig. S3 to S42 Congener group patterns of CPs for all samples, the y-axis represents the internal standard corrected instrument response, red bars represent SCCPs, the green for MCCPs and the blue for LCCPs

Materials. Seven commercially available CP standard mixtures C₁₀-C₁₃ (SCCP 51.5%Cl), C₁₀-C₁₃ (SCCP 55.5%Cl), C₁₄-C₁₇ (MCCP 42%Cl), C₁₄-C₁₇ (MCCP 52%Cl), C₁₄-C₁₇ (MCCP 57%Cl), C₁₈-C₂₀ (LCCP 36%Cl), C₁₈-C₂₀ (LCCP 49%Cl), and ¹³C₁₀-anti-Dechlorane Plus® (¹³C₁₀-anti-DP) were purchased from Dr. Ehrenstorfer GmbH (Augsburg, Germany). Dust standard reference material (SRM 2585) was purchased from The National Institute of Standards and Technology (NIST) (Gaithersburg, MD, USA). The solvents and chemicals used were all analytical or HPLC grade, unless otherwise stated. Dichloromethane (DCM), methanol, acetone, and n-hexane were purchased from J.T Baker, Deventer, The Netherlands. Whatman® grade 541 filter paper, silica gel, and Florisil® were purchased from Sigma-Aldrich (now Merck), Amsterdam, The Netherlands.

Table S1. Details on samples associated with vacuum cleaner bags (VD), freshly collected dust (FD) and cat hair (CH)

	VD	FD	C-hair
House 1	VD-1	FD-1	CH-1A, CH-1B
House 2	VD-2	FD-2	CH-2A, CH-2B, CH-2C, CH-2D
House 3	VD-3	FD-3	CH-3
House 4	VD-4	FD-4	CH-4A, CH-4B
House 5	VD-5	FD-5	CH-5
House 6	VD-6	FD-6	CH-6
House 7	VD-7	FD-7	
House 8	VD-8	FD-8	
House 9	VD-9	FD-9	
House 10	VD-10	FD-10	
House 11	VD-11		

Quadrupole time-of-flight mass spectrometry (qTOF-MS) settings: The atmospheric pressure chemical ionization (APCI) source parameters included: vaporizer and drying gas temperatures of 300°C and 200°C respectively, and nitrogen gas flow rates of 2.0 L/min for the nebulizer and drying gas. The capillary voltage was set at 2.0 eV and the corona current at 6000 nA. The qTOF-MS was operated in negative ion mode and full scan data was collected from *m/z* 200 to 1500 at a resolution of 25,000 FWHM (full width at half maximum). Internal mass calibration was performed by introducing the Agilent APCI-L low concentration tuning mix (part No: G1969-85010). The standard deviation for the mass calibration was better than 0.3 ppm. The total analysis run time was 4 minutes.

Table S2. Theoretical *m/z* ratios and isotopic abundances ratios of quantitation and qualifier [M+Cl]⁻ ions for CPs.

Formula [M+Cl] ⁻	Quan ion	Qual ion	Ratio (%)	Formula [M+Cl] ⁻	Quan ion	Qual ion	Ratio (%)	Formula [M+Cl] ⁻	Quan ion	Qual ion	Ratio (%)
C9H17Cl3	267.0061	265.0090	77.9	C24H43Cl7	615.0822	613.0850	87.8	C32H47Cl19	1140.7312	1138.7340	96.3
C9H16Cl4	300.9671	302.9642	64.3	C24H42Cl8	649.0432	647.0460	77.0	C32H46Cl20	1174.6922	1172.6950	90.7
C9H15Cl5	334.9281	336.9252	80.2	C24H41Cl9	683.0042	685.0014	86.7	C32H45Cl21	1208.6532	1210.6504	91.9
C9H14Cl6	368.8891	370.8862	96.2	C24H40Cl10	716.9652	718.9624	97.3	C32H44Cl22	1242.6142	1244.6113	97.2
C9H13Cl7	404.8472	402.8502	89.1	C24H39Cl11	752.9234	750.9262	92.6	C32H43Cl23	1278.5723	1276.5752	97.5
C9H12Cl8	438.8083	436.8112	78.0	C24H38Cl12	786.8844	784.8873	84.3	C32H42Cl24	1312.5333	1310.5362	92.7
C9H11Cl9	472.7693	474.7664	85.5	C24H37Cl13	820.8454	822.8426	89.0	C32H41Cl25	1346.4943	1348.4915	92.5
C10H19Cl3	281.0217	279.0246	77.8	C24H36Cl14	854.8064	856.8036	97.0	C32H40Cl26	1380.4554	1382.4525	97.0
C10H18Cl4	314.9828	316.9799	64.3	C24H35Cl15	890.7646	888.7674	95.3	C32H39Cl27	1416.4135	1414.4164	98.4
C10H17Cl5	348.9438	350.9409	80.3	C24H34Cl16	924.7256	922.7284	88.5	C32H38Cl28	1450.3745	1448.3774	94.2
C10H16Cl6	382.9048	384.9019	96.3	C24H33Cl17	958.6866	960.6837	90.4	C32H37Cl29	1484.3355	1486.3327	92.9
C10H15Cl7	418.8629	416.8658	89.1	C24H32Cl18	992.6476	994.6447	96.8	C33H65Cl3	603.3821	601.3846	74.4
C10H14Cl8	452.8239	450.8268	78.0	C24H31Cl19	1028.6057	1026.6086	96.9	C33H64Cl4	637.3430	639.3406	67.7

C22H39CI7	587.0509	585.0537	88.1	C31H59CI5	643.2727	645.2701	83.2	C39H67CI13	1031.0806	1033.0779	90.7
C22H38CI8	621.0119	619.0147	77.2	C31H58CI6	677.2337	679.2310	99.2	C39H66CI14	1065.0415	1067.0388	98.6
C22H37CI9	654.9729	656.9701	86.4	C31H57CI7	713.1920	711.1947	86.9	C39H65CI15	1100.9998	1099.0025	93.8
C22H36CI10	688.9339	690.9311	97.1	C31H56CI8	747.1529	749.1503	76.9	C39H64CI16	1134.9608	1132.9635	87.3
C22H35CI11	724.8921	722.8949	92.8	C31H55CI9	781.1139	783.1112	87.6	C39H63CI17	1168.9218	1170.9190	91.7
C22H34CI12	758.8531	756.8559	84.5	C31H54CI10	815.0749	817.0722	98.2	C39H62CI18	1202.8827	1204.8800	98.1
C22H33CI13	792.8141	794.8112	88.8	C31H53CI11	851.0332	849.0359	91.9	C39H61CI19	1238.8410	1236.8437	95.7
C22H32CI14	826.7751	828.7722	96.8	C31H52CI12	884.9941	882.9969	83.7	C39H60CI20	1272.8020	1270.8047	90.2
C22H31CI15	862.7332	860.7361	95.4	C31H51CI13	918.9551	920.9524	89.7	C39H59CI21	1306.7629	1308.7602	92.5
C22H30CI16	896.6942	894.6971	88.6	C31H50CI14	952.9161	954.9133	97.7	C39H58CI22	1340.7239	1342.7212	97.8
C22H29CI17	930.6552	932.6524	90.3	C31H49CI15	988.8743	986.8771	94.7	C39H57CI23	1376.6821	1374.6849	97.0
C22H28CI18	964.6163	966.6134	96.7	C31H48CI16	1022.8353	1020.8381	88.0	C39H56CI24	1410.6431	1408.6459	92.2
C22H27CI19	1000.5744	998.5773	97	C31H47CI17	1056.7963	1058.7935	91.0	C39H55CI25	1444.6041	1446.6013	93.0
C22H26CI20	1034.5354	1032.5383	91.4	C31H46CI18	1090.7573	1092.7545	97.3	C39H54CI26	1478.5651	1480.5623	97.5
C22H25CI21	1068.4964	1070.4935	91.2	C31H45CI19	1126.7155	1124.7183	96.4	C40H79CI3	701.4919	699.4941	72.7
C22H24CI22	1102.4574	1104.4545	96.6	C31H44CI20	1160.6765	1158.6793	90.8	C40H78CI4	735.4528	737.4506	69.5
C23H45CI3	463.2254	461.2281	76.3	C31H43CI21	1194.6375	1196.6347	91.8	C40H77CI5	769.4137	771.4113	85.3
C23H44CI4	497.1864	499.1837	65.8	C31H42CI22	1228.5985	1230.5957	97.1	C40H76CI6	805.3722	803.3747	98.8
C23H43CI5	531.1474	533.1446	81.8	C31H41CI23	1264.5567	1262.5595	97.6	C40H75CI7	839.3331	837.3356	85.3
C23H42CI6	565.1084	567.1056	97.7	C31H40CI24	1298.5177	1296.5205	92.8	C40H74CI8	873.2941	875.2916	78.4
C23H41CI7	601.0666	599.0694	88	C31H39CI25	1332.4787	1334.4758	92.4	C40H73CI9	907.2550	909.2524	89.0
C23H40CI8	635.0276	633.0304	77.1	C31H38CI26	1366.4397	1368.4368	97.0	C40H72CI10	941.2160	943.2134	99.6
C23H39CI9	668.9886	670.9857	86.5	C31H37CI27	1402.3978	1400.4007	98.5	C40H71CI11	977.1743	975.1770	90.7
C23H38CI10	702.9496	704.9467	97.2	C31H36CI28	1436.3588	1434.3617	94.3	C40H70CI12	1011.1353	1013.1326	82.8
C23H37CI11	738.9077	736.9106	92.7	C31H35CI29	1470.3198	1472.3170	92.9	C40H69CI13	1045.0962	1047.0936	90.8
C23H36CI12	772.8687	770.8716	84.4	C32H63CI3	589.3664	587.3689	74.6	C40H68CI14	1079.0572	1081.0545	98.8
C23H35CI13	806.8297	808.8269	88.9	C32H62CI4	623.3274	625.3249	67.5	C40H67CI15	1115.0155	1113.0182	93.7
C23H34CI14	840.7908	842.7879	96.9	C32H61CI5	657.2883	659.2858	83.4	C40H66CI16	1148.9765	1146.9792	87.2
C23H33CI15	876.7489	874.7518	95.3	C32H60CI6	691.2493	693.2467	99.4	C40H65CI17	1182.9374	1184.9347	91.9
C23H32CI16	910.7099	908.7128	88.6	C32H59CI7	727.2077	725.2103	86.7	C40H64CI18	1216.8984	1218.8957	98.2
C23H31CI17	944.6709	946.6680	90.3	C32H58CI8	761.1686	763.1660	77.1	C40H63CI19	1252.8567	1250.8594	95.6
C23H30CI18	978.6319	980.6291	96.7	C32H57CI9	795.1296	797.1269	87.7	C40H62CI20	1286.8177	1284.8204	90.1
C23H29CI19	1014.5901	1012.5929	97	C32H56CI10	829.0906	831.0879	98.3	C40H61CI21	1320.7786	1322.7759	92.6
C23H28CI20	1048.5511	1046.5540	91.3	C32H55CI11	865.0488	863.0516	91.8	C40H60CI22	1354.7396	1356.7369	97.9
C23H27CI21	1082.5121	1084.5092	91.3	C32H54CI12	899.0098	897.0126	83.6	C40H59CI23	1390.6978	1388.7006	96.9
C23H26CI22	1116.4731	1118.4702	96.6	C32H53CI13	932.9708	934.9681	89.8	C40H58CI24	1424.6588	1422.6616	92.2
C23H25CI23	1152.4312	1150.4341	98.1	C32H52CI14	966.9318	968.9290	97.8	C40H57CI25	1458.6198	1460.6170	93.0
C24H47CI3	477.2410	475.2437	76.1	C32H51CI15	1002.8900	1000.8928	94.6	C40H56CI26	1492.5808	1494.5780	97.6
C24H46CI4	511.2020	513.1994	66	C32H50CI16	1036.8510	1034.8538	87.9				
C24H45CI5	545.1630	547.1603	81.9	C32H49CI17	1070.8120	1072.8092	91.1				
C24H44CI6	579.1240	581.1213	97.9	C32H48CI18	1104.7730	1106.7702	97.4				

Table S3. Calculated degree of chlorination for the Σ SCCP, Σ MCCP and Σ LCCP technical mixtures

Technical mixture	Calculated Cl-degree
SCCP (51.5 %)	55.5%
SCCP (55.5 %)	57.8%
MCCP (42 %)	49.3%
MCCP (52 %)	54.1%
MCCP (57 %)	57.4%
LCCP (36 %)	38.2%
LCCP (49 %)	49.3%

Table S4. Total Σ SCCPs, Σ MCCPs and Σ LCCPs concentration in $\mu\text{g/g}$ measured in the dust reference material (SRM 2585) with the degree of chlorination. The goodness of fit (R^2) below 0.5 are given in *italic* and highlighted red with indicated that the reported values are tentative.

Sample	SCCP ($\mu\text{g/g}$)	R^2	Cl %	MCCP ($\mu\text{g/g}$)	R^2	Cl %	LCCP ($\mu\text{g/g}$)	R^2	Cl %
NIST 2585(1)	8.5	0.8	59%	11.9	0.7	52%	19.1	<0.1	40%
NIST 2585(2)	8.6	0.8	59%	11.6	0.7	52%	18.1	<0.1	40%
NIST 2585(3)	8.9	0.8	59%	12.4	0.7	52%	19.6	<0.1	40%
NIST 2585(4)	8.8	0.8	59%	11.9	0.7	52%	19.0	<0.1	40%
NIST 2585(5)	8.5	0.8	59%	11.7	0.7	52%	19.0	<0.1	40%
NIST 2585(6)	8.9	0.8	59%	12.0	0.7	52%	19.6	<0.1	40%
NIST 2585(7)	8.6	0.8	59%	12.2	0.7	52%	20.1	<0.1	40%
NIST 2585(8)	8.5	0.8	59%	12.1	0.7	52%	19.6	<0.1	40%
NIST 2585(9)	8.5	0.8	59%	12.1	0.7	52%	19.2	<0.1	39%

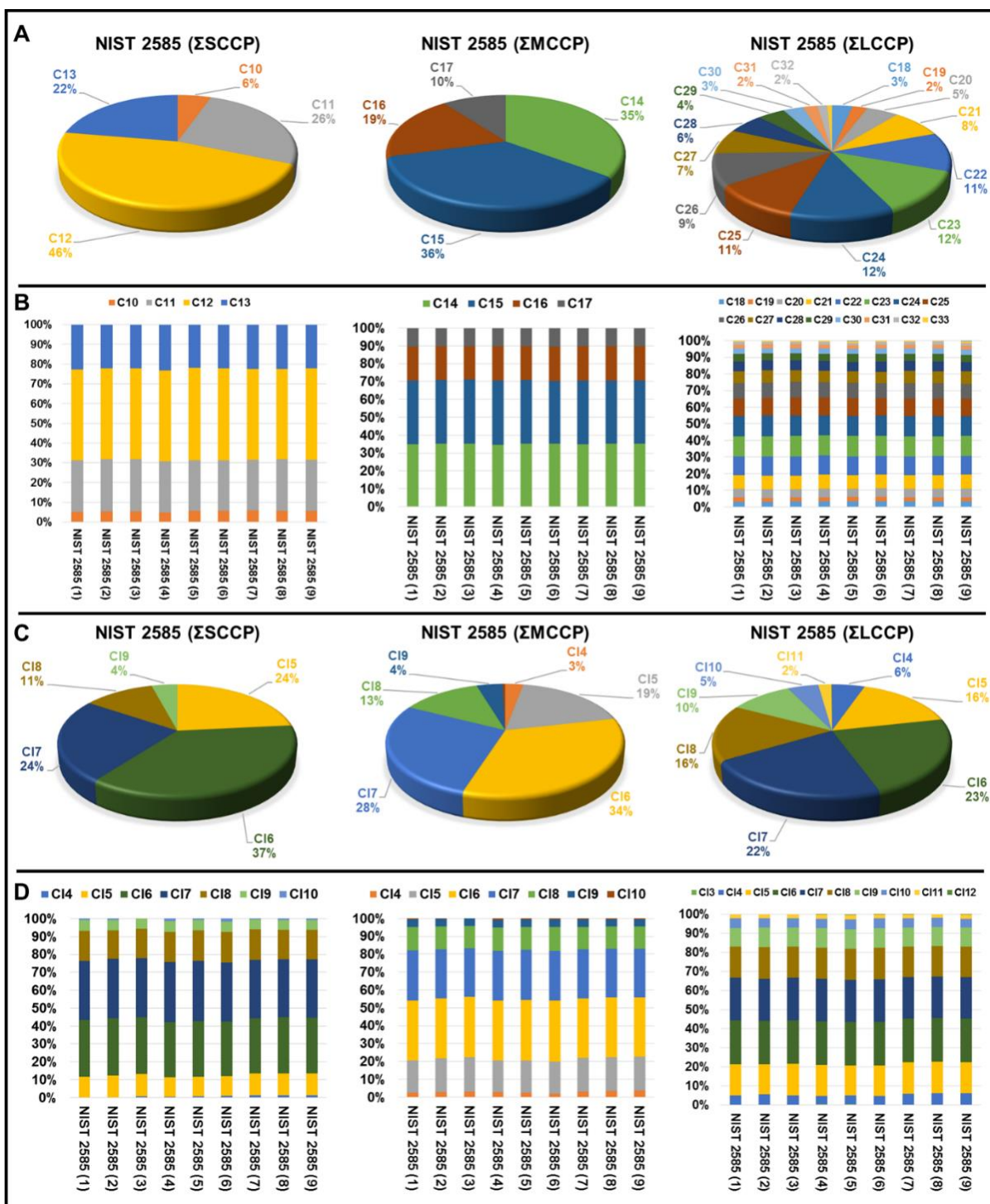


Fig. S1. Composition of CPs in the dust reference material (SRM 2585) (A), Σ SCCP, Σ MCCP, and Σ LCCP composition based on carbon chain length, (B) Σ SCCP, Σ MCCP, and Σ LCCP carbon chain length in the repeat measurements, (C) Σ SCCP, Σ MCCP, and Σ LCCP composition based on chlorine substitution, (D) Σ SCCP, Σ MCCP, and Σ LCCP chlorine substitution in the repeat measurements.

The use of non-traditional Kendrick MD plots for the identification of CP congeners. An average full scan mass spectrum of the chromatographic peaks was extracted using Bruker Compass DataAnalysis software and the accurate mass list was exported to Microsoft Excel. The non-traditional

Kendrick MD plots were constructed by converting the measured IUPAC m/z to $[-H/+Cl]$ mass scales corresponding to the mass of a chlorine atom minus the mass of a hydrogen atom.

$$\text{Accurate H/Cl scaled mass} = \text{Accurate mass (IUPAC mass)} \times \left(\frac{34}{33.961028} \right)$$

$$\text{H/Cl scaled mass defect} = \text{nominal mass (rounded)} - \text{accurate H/Cl scaled mass}$$

As shown in Fig. S2, the Kendrick MD plots are graphically constructed as bubble plots by positioning the accurate masses on the x-axis and the corresponding H/Cl scaled mass defects on the y-axis with peak intensity as the bubble size. The CP congeners with the same carbon chain length (C_9 to C_{40}) and increased degree of substitution ($Cl_3 <$) are positioned on horizontal lines separated by H/Cl substitution. The congeners with the same degree of substitution and increased carbon chain length are positioned on diagonal lines. The coloured spheres in the Kendrick MD plots represent the quantifier and qualifier $[M+Cl]^+$ ions for SCCPs (red), MCCPs (green) and LCCPs (blue) which were positively identified based on the criteria discussed in the quantitation and deconvolution section. To briefly explain the outlay of the plot using C_{19} -congeners as an example, the $[M+Cl]^+$ IUPAC masses for $C_{19}H_{34}Cl_6$, $C_{19}H_{33}Cl_7$, and $C_{19}H_{32}Cl_8$ are 507.0486, 541.0096, and 574.9706 respectively. These masses are then converted to the H/Cl scaled masses, resulting in 507.6304, 541.6304, and 575.6304. By subtracting the new accurate H/Cl scaled mass from the rounded nominal mass, the H/Cl scaled mass defect for all three C_{19} -congeners is 0.6304. As shown in the enlarged region in Fig. S2B, these C_{19} -congeners are positioned on a horizontal line separated by H/Cl substitution. The CP congeners with carbon chains C_{31} to C_{40} appear at the bottom of the plot resulting in “wrap-around” due to the increase in mass defect as a result of the high proportion of hydrogen atoms. For example, when the IUPAC masses for $C_{30}H_{59}Cl_3$ (559.3376) and $C_{31}H_{61}Cl_3$ (573.3533) are converted to the respective H/Cl scaled masses, the new accurate H/Cl scaled masses are 559.9795 and 574.0112. The H/Cl scaled mass defect for $C_{30}H_{59}Cl_3$ is 0.9795, which are positioned at the top of the plot, and $C_{31}H_{61}Cl_3$ is 0.0112 which “wrap-around” to be positioned at the bottom of the plot.

As shown in Fig. S2B and S2C, the pattern observed for the VD-6 differs from the pattern observed for VD 2, where more abundant C_{19} and congeners $>C_{29}$ were observed. The enlarged section shows the difference between measured and theoretical masses for the C_{19} homologue group ($C_{19}H_{35}Cl_5$ to $C_{19}H_{28}Cl_{12}$) depicted as black circles. The accurate masses for these congeners were within 10 ppm of the theoretical masses, but the ion ratios varied by more than 40% from the theoretical ion ratios (Fig. S3). This was also observed for the CP congeners with carbon lengths of C_{30} and longer. This emphasises the use of strict mass accuracy criteria and the use of ion pair intensity ratios to distinguish between positive identified CPs and the presence of possible interferences. This pattern was also observed for the cat hair (CH-6) taken from the same household.

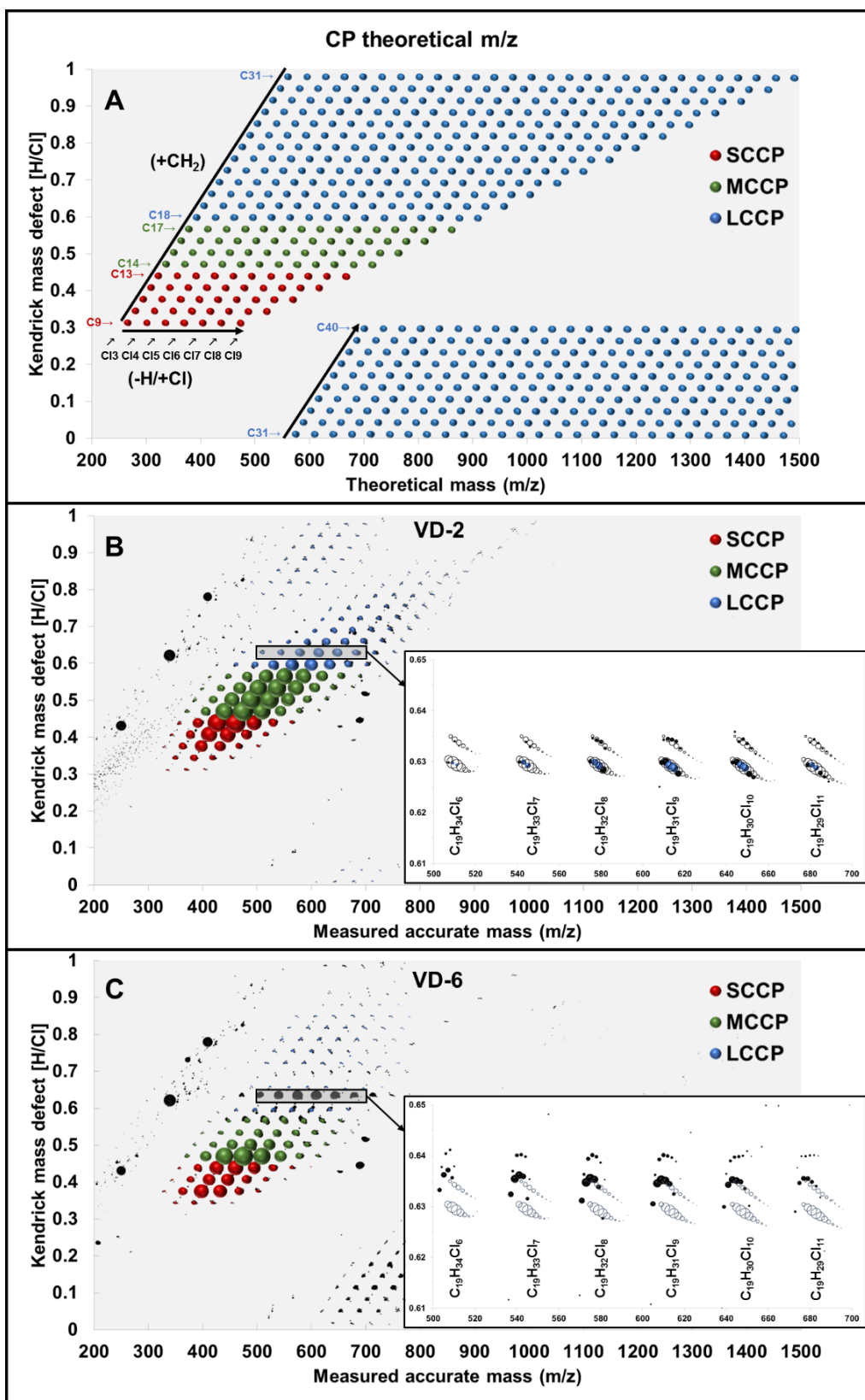


Fig. S2. Non-traditional Kendrick MD plots, (A) constructed from the theoretical m/z quantitation and qualifier $[M+Cl]^-$ ions for CPs listed in Table S1 (see text below for detailed explanation), (B) constructed for VD-2, (C) and VD-6. The red spheres represent the quantifier and qualifier $[M+Cl]^-$ ions for SCCPs, the green for MCCPs and the blue for LCCPs the sphere size represent the instrument response. The enlarged region shows the theoretical m/z and ion intensity ratios for C₁₉H₃₄Cl₆ to C₁₉H₂₉Cl₁₁ depicted as black circles.

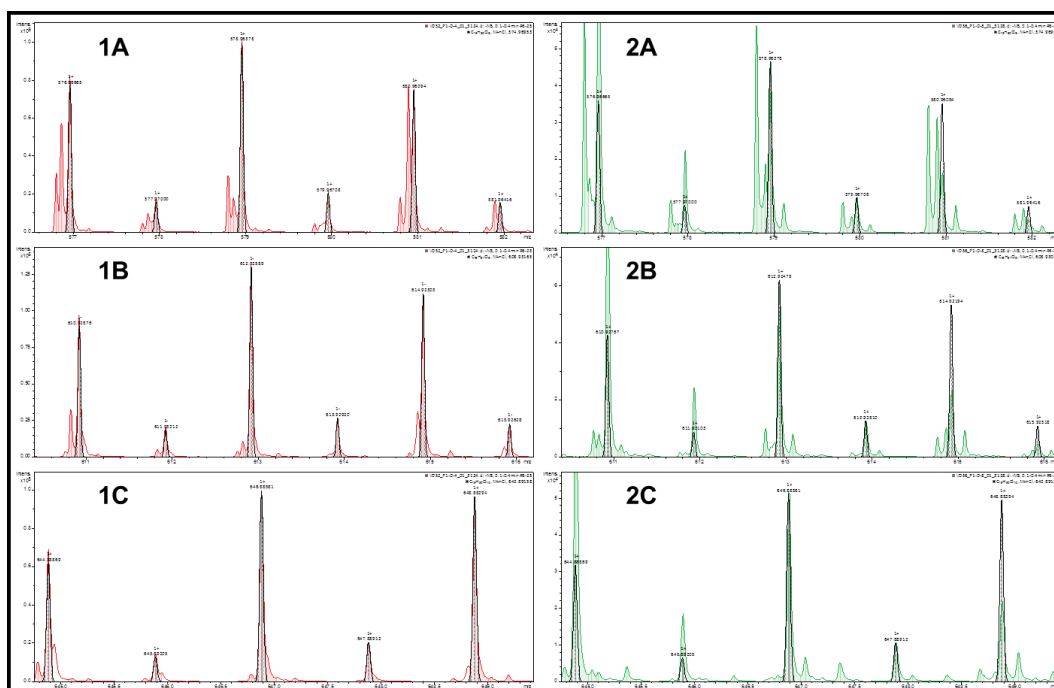


Fig. S3. Negative ion APCI-qTOF-MS mass scale-expanded segments of the mass spectra extracted for (A) C₁₉H₃₂Cl₈, (B) C₁₉H₃₁Cl₉, and (C) C₁₉H₃₀Cl₁₀ from (1) VD-2 in red and (2) VD-6 in green. The black profile represents the mass spectra for the theoretical [M+Cl]⁻ ions of the respective congeners. This figure emphasises the ion ratio deviation observed for VD-6

Table S5. Total ΣSCCPs, ΣMCCPs, and ΣLCCPs concentration in µg/g for VD, FD and CH with the degree of chlorination. The goodness of fit (R²) below 0.5 are given in *Italic* and highlighted red with indicated that the reported values are tentative.

Sample	SCCP (µg/g)	R ²	Cl %	MCCP (µg/g)	R ²	Cl %	LCCP (µg/g)	R ²	Cl %
VD-1	19	0.8	58%	34	0.9	54%	4.3	0.7	50%
VD-2	214	0.8	58%	200	0.5	56%	74	<i>0.4</i>	54%
VD-3	8.6	0.7	57%	13	0.9	55%	23	<i>0.1</i>	50%
VD-4	58	0.6	59%	86	0.9	56%	14	0.5	52%
VD-5	14	0.6	59%	46	0.9	55%	7.7	0.6	48%
VD-6	136	0.8	59%	84	1.0	56%	8.6	0.5	48%
VD-7	10	0.6	59%	40	0.8	55%	13	<i>0.4</i>	43%
VD-8	5.1	0.5	58%	16	0.9	55%	14	<i><0.1</i>	38%
VD-9	12	0.7	58%	54	0.8	55%	8.8	0.7	48%
VD-10	7.5	0.7	59%	22	0.9	55%	6.2	0.6	46%
VD-11	44	0.7	59%	165	0.8	55%	19	0.7	51%
FD-1	9.3	0.7	59%	21	0.9	55%	2.5	0.5	51%
FD-2	25	0.7	58%	47	0.8	55%	24	<i>0.2</i>	39%
FD-3	30	0.6	58%	62	0.9	55%	1.9	0.5	51%
FD-4	93	0.6	57%	259	0.9	55%	28	0.7	52%
FD-5	353	0.8	58%	283	0.9	56%	27	0.5	53%
FD-6	10	0.6	56%	498	0.6	56%	108	0.8	52%
FD-8	5.4	0.7	58%	46	0.8	55%	9.4	0.8	47%
FD-9	12	0.7	58%	29	0.9	55%	5.9	0.6	48%
FD-10	17	0.6	59%	36	0.9	55%	7.2	0.7	49%
CH-1A	1.5	0.6	59%	4.6	0.7	56%	0.9	0.6	53%
CH-1B	2.0	0.7	59%	4.0	0.9	56%	0.7	0.5	53%
CH-2A	3.0	0.8	58%	5.8	0.9	55%	2.3	<i>0.1</i>	38%
CH-2B	1.7	0.7	59%	2.6	0.9	55%	1.0	<i>0.4</i>	43%
CH-2C	2.4	0.8	58%	3.2	0.9	54%	1.6	<i>0.1</i>	37%
CH-2D	2.0	0.7	58%	3.2	0.9	55%	0.9	<i>0.4</i>	42%
CH-3	0.5	0.7	57%	0.6	0.9	54%	0.1	0.5	50%
CH-4A	7.2	0.7	58%	6.5	1.0	55%	0.9	0.5	52%
CH-4B	6.2	0.8	58%	4.7	1.0	55%	0.6	0.6	52%
CH-5	2.2	0.5	57%	4.8	1.0	55%	0.8	0.5	47%
CH-6	0.8	0.7	57%	1.4	0.9	54%	0.2	0.6	48%

Table S6. Comparisons of Σ SCCP, Σ MCCP and Σ LCCP concentrations ($\mu\text{g/g}$) in indoor dust.

Country	Dust type	Σ SCCP ($\mu\text{g/g}$)	Σ MCCP ($\mu\text{g/g}$)	Σ LCCP ($\mu\text{g/g}$)	Reference
		Median (Range)	Median (Range)	Median (Range)	
Sweden	Apartment	7.5 (3.2 - 18.0)			(Fridén et al., 2011)
Germany (n=11)	House	5 (4 - 27)	176 (9 - 892)		(Hilger et al., 2013)
Taiwan (n=5)	House & office	(1.2 - 31.2)			(Chen et al., 2016)
China (n=14)	Building material mall	76.7 (6.0 - 361.4)	101.7 (5.0 - 285.9)		(Shi et al., 2017)
Australia (n=1)	Office	61	180	99	(Wong et al., 2017)
Canada (n=4)	Office	55 (22 - 65)	185 (140 - 192)	134 (92 - 161)	(Wong et al., 2017)
China (n=5)	Office	580 (106 - 808)	1398 (330 - 1948)	1432 (153 - 1995)	(Wong et al., 2017)
Sweden (n=3)	Office	7 (5 - 9)	101 (67 - 158)	710 (567 - 1264)	(Wong et al., 2017)
UK (n=1)	House	93	463	157	(Wong et al., 2017)
China (n=30)	Apartment	44.1 (10.1 - 158.2)			(Liu et al., 2017)
China (n=5)	Office	50.9 (40.5 - 80.6)			(Liu et al., 2017)
China (n=22)	Commercial store	53.8 (13.3 - 173)			(Liu et al., 2017)
China (n=15)	House	46.5 (27.8 - 173)	166 (74 - 539)		(Chen et al., 2018)
China (n=30)	Houses near E-waste	412 (34.5 - 2030)	1250 (79.2 - 6510)		(Chen et al., 2018)
China (n=20)	Apartment & office	(0 - 171)			(Huang et al., 2018)
China (n=115)	House	98.7 (5.35 - 1022)	89.8 (2.10 - 725)		(Gao et al., 2018)
Canada (n=48)	House	6.2 (4 - 57)	19 (5.9 - 901.0)		(Shang et al., 2019)
Australia (n=27)	House	13* (1.0 - 42)	46 (8.8 - 380)	3.0* (<0.0014 - 15)	(He et al., 2019)
South Africa (n=20)	House	16 (5.1 - 353)	46 (13 - 498)	11 (1.9 - 108)	This study

*Average

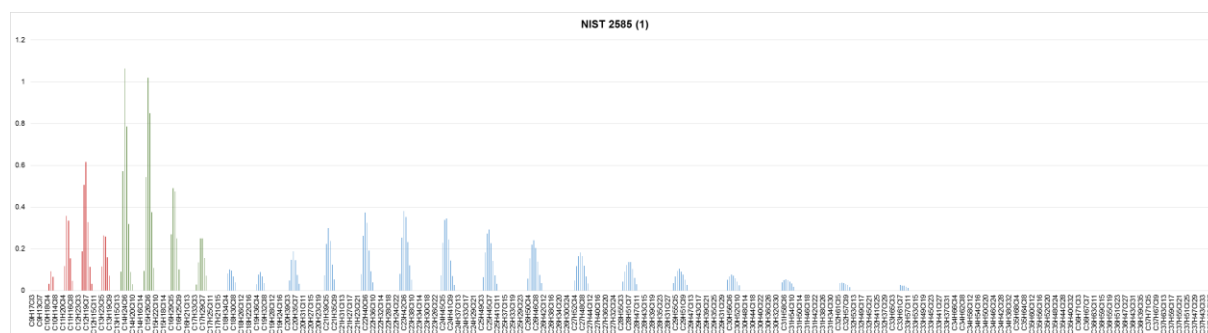


Fig. S4. Congener group patterns of CPs for NIST 2585 (1)

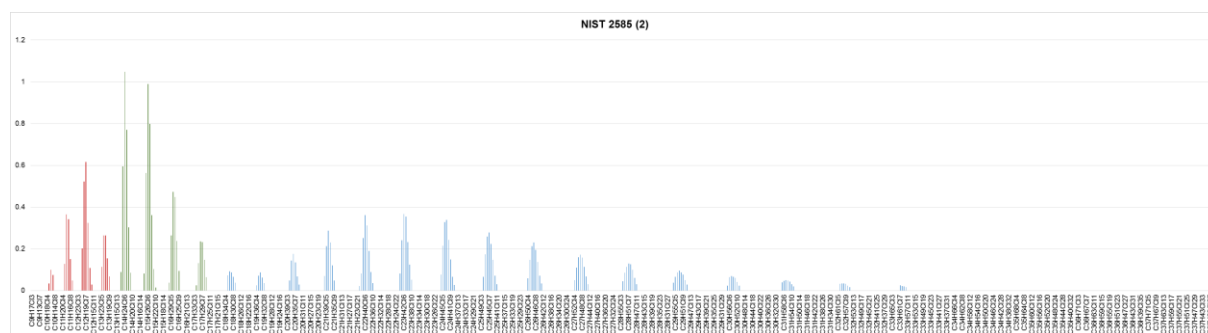


Fig. S5. Congener group patterns of CPs for NIST 2585 (2)

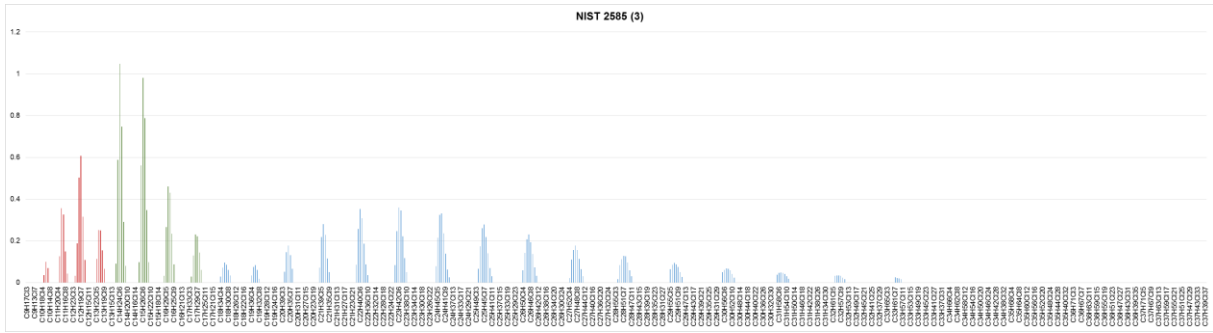


Fig. S6. Congener group patterns of CPs for NIST 2585 (3)

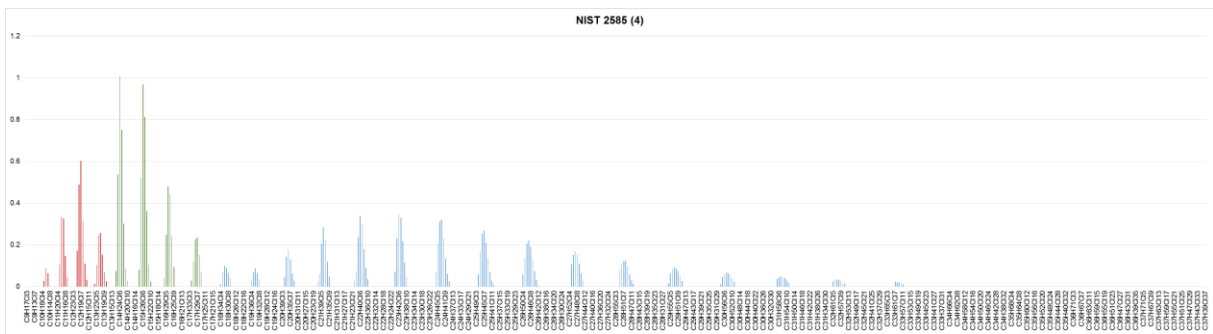


Fig. S7. Congener group patterns of CPs for NIST 2585 (4)

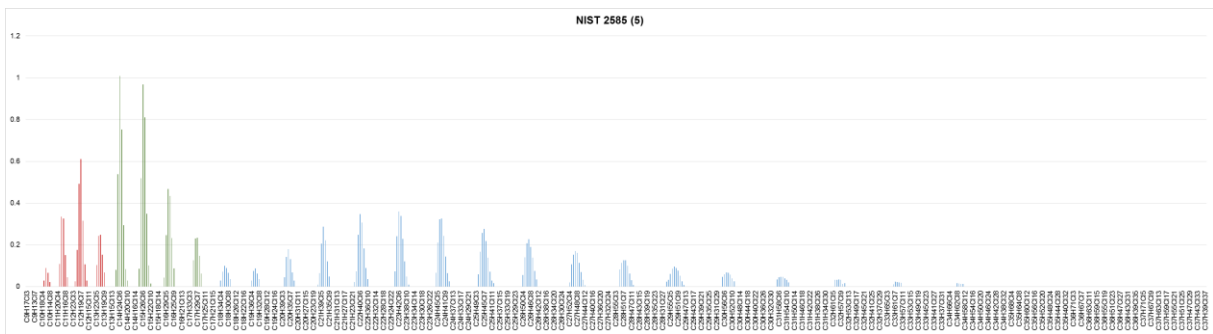


Fig. S8. Congener group patterns of CPs for NIST 2585 (5)

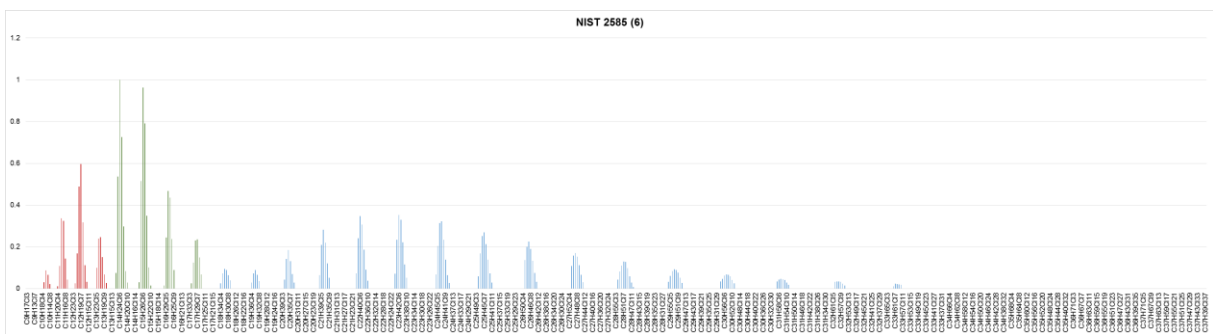


Fig. S9. Congener group patterns of CPs for NIST 2585 (6)

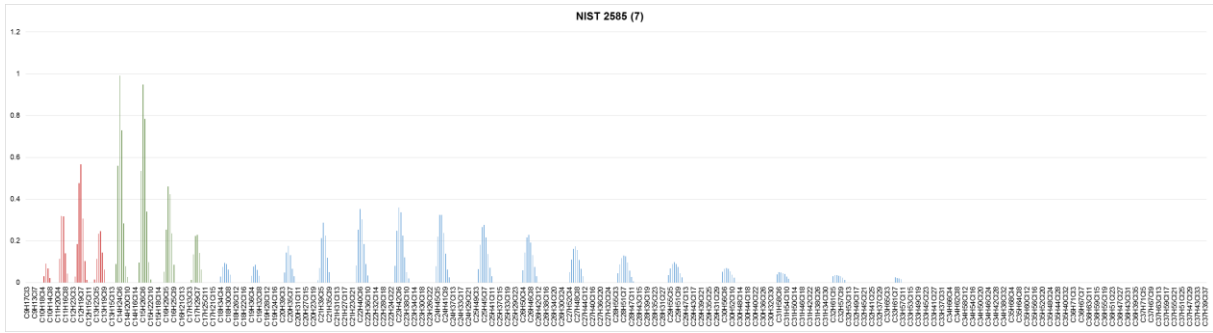


Fig. S10. Congener group patterns of CPs for NIST 2585 (7)

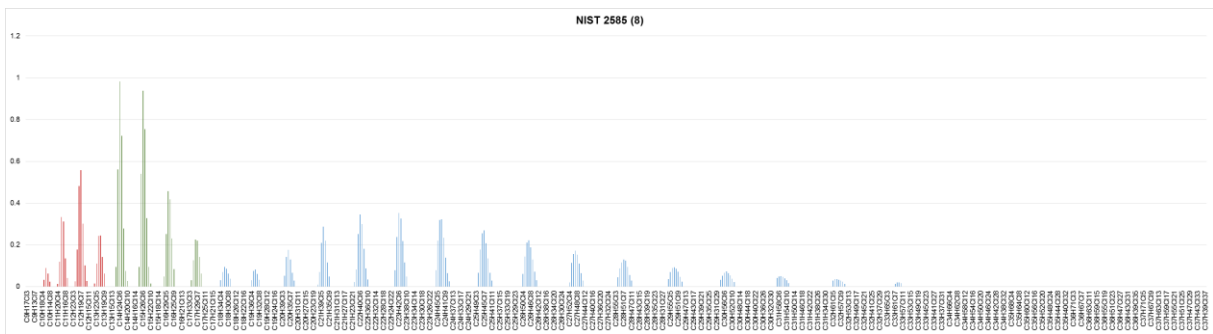


Fig. S11. Congener group patterns of CPs for NIST 2585 (8)

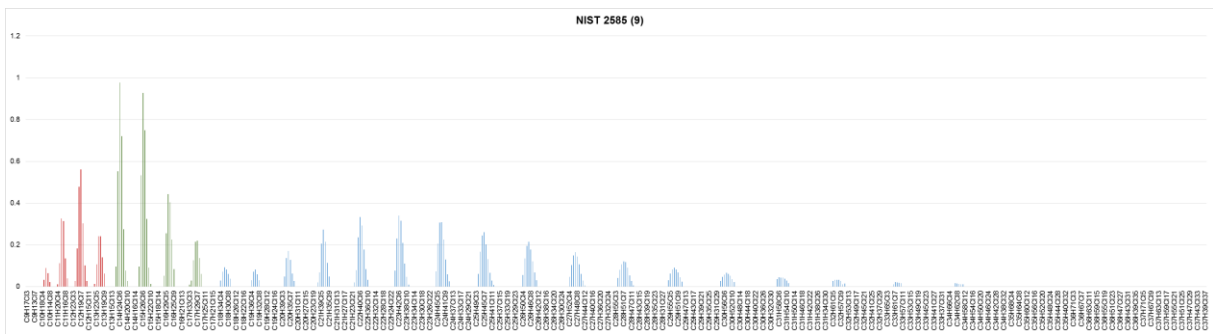


Fig. S12. Congener group patterns of CPs for NIST 2585 (9)

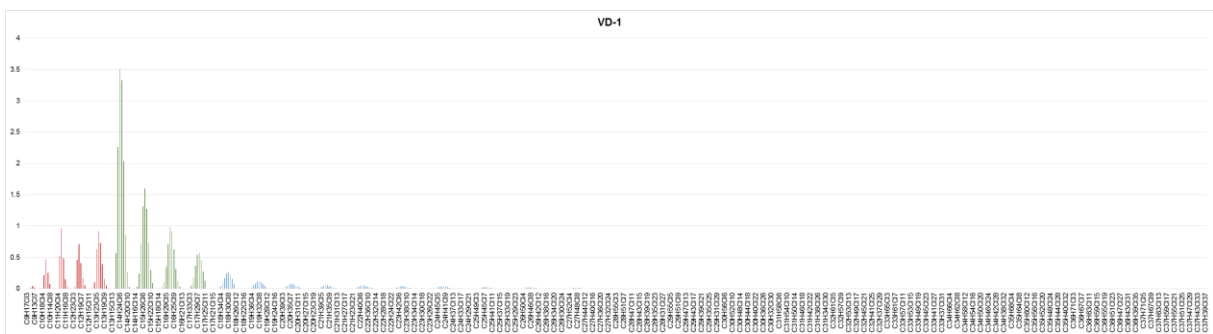


Fig. S13. Congener group patterns of CPs for VD-1

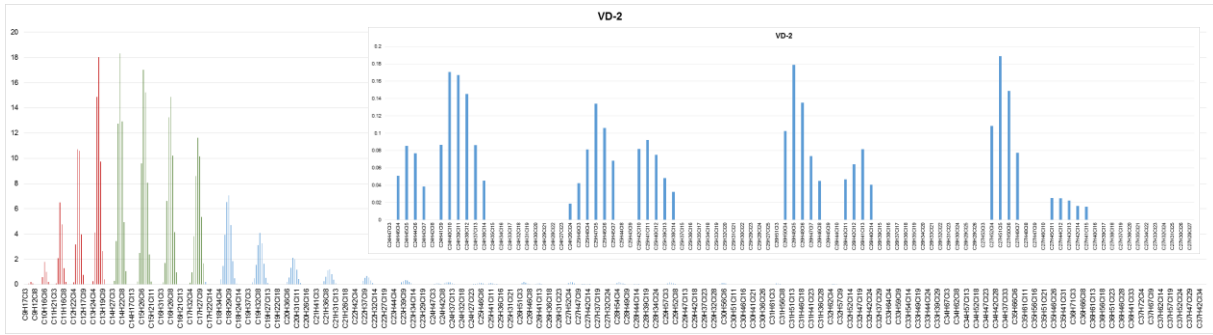


Fig. S14. Congener group patterns of CPs for VD-2, the enlarged region show the double chlorination peak observed for C₂₄ to C₂₇

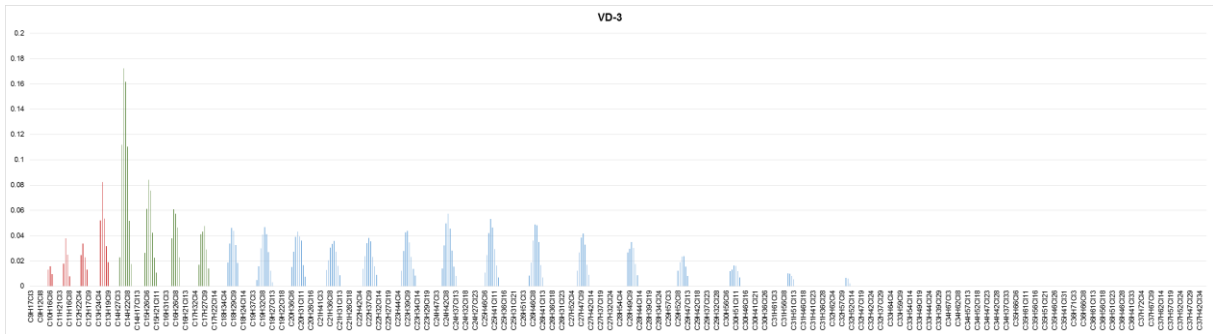


Fig. S15. Congener group patterns of CPs for VD-3

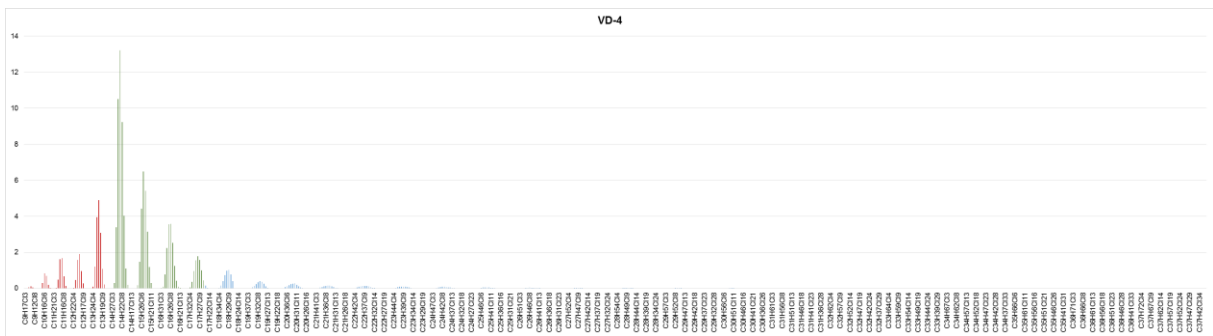


Fig. S16. Congener group patterns of CPs for VD-4

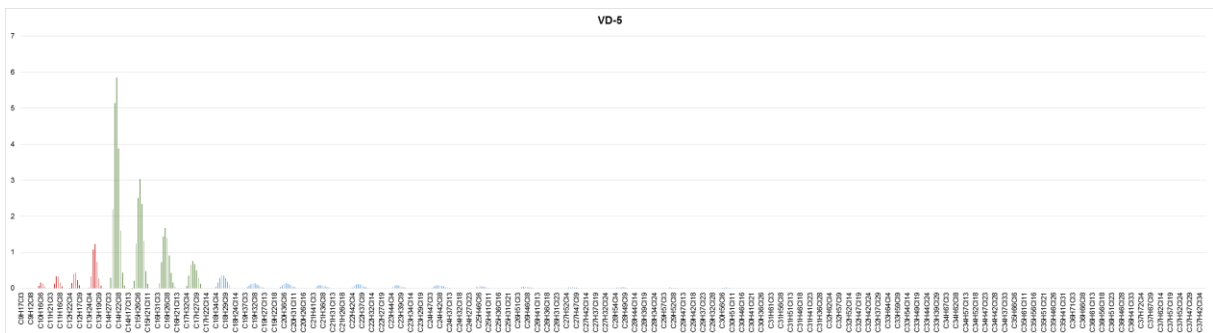


Fig. S17. Congener group patterns of CPs for VD-5

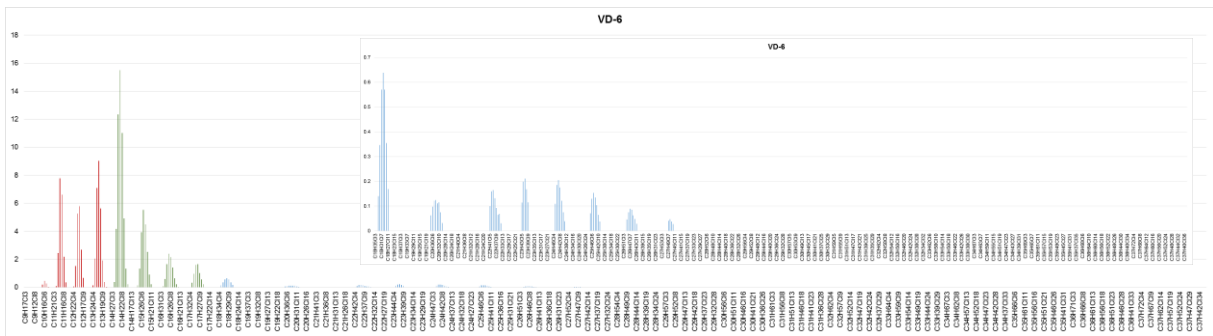


Fig. S18. Congener group patterns of CPs for VD-6, the enlarged region show the pattern for C₁₈ to C₃₇

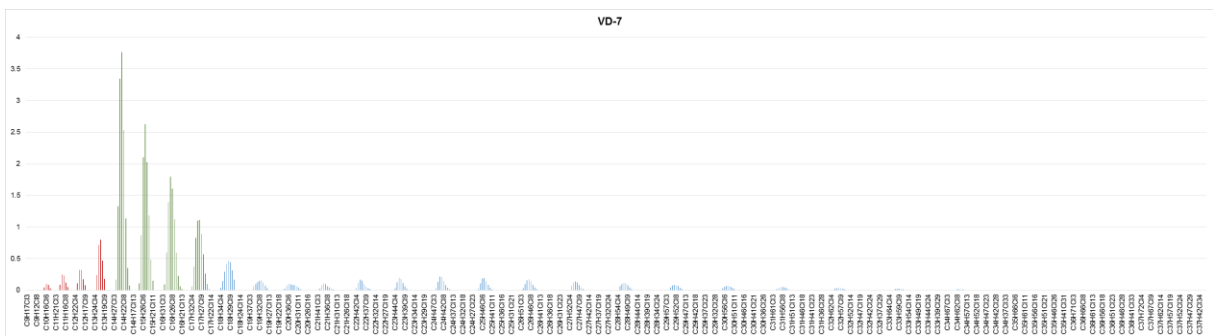


Fig. S19. Congener group patterns of CPs for VD-7

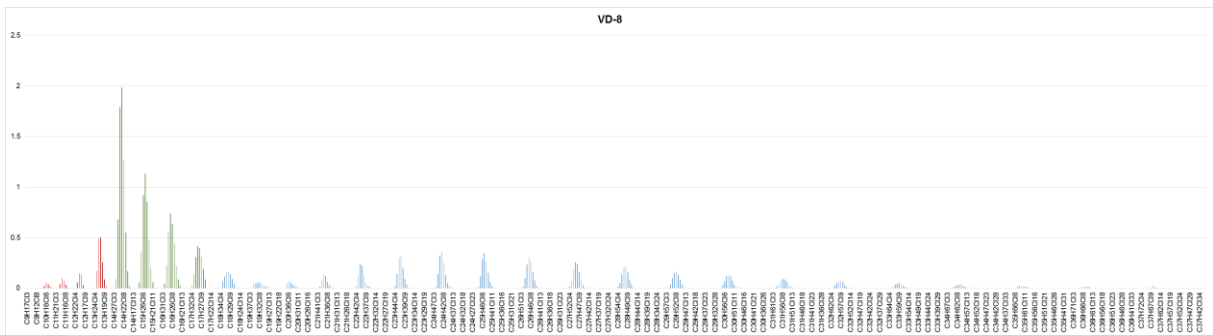


Fig. S20. Congener group patterns of CPs for VD-8

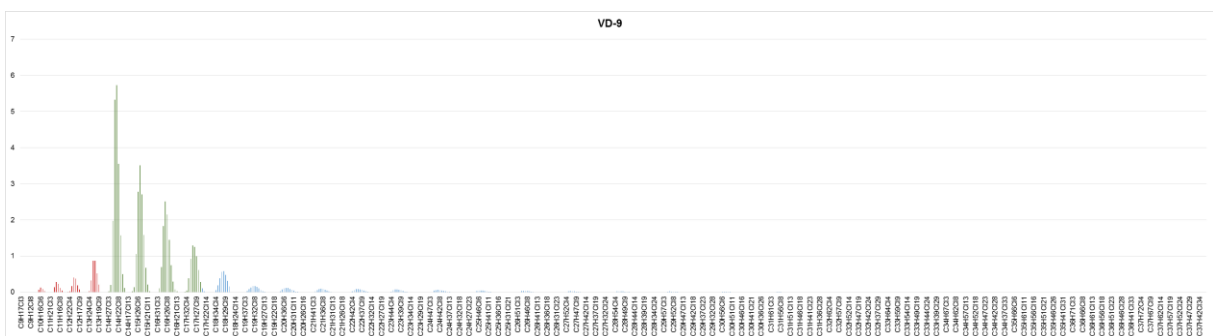


Fig. S21. Congener group patterns of CPs for VD-9

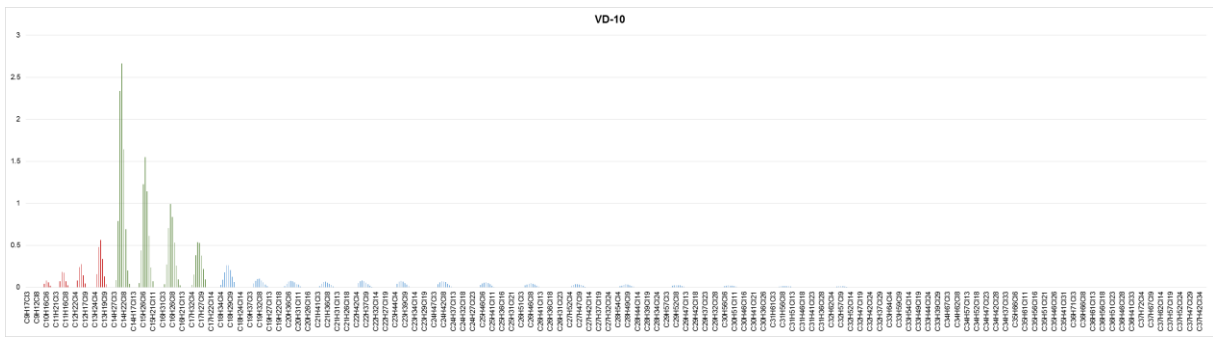


Fig. S22. Congener group patterns of CPs for VD-10

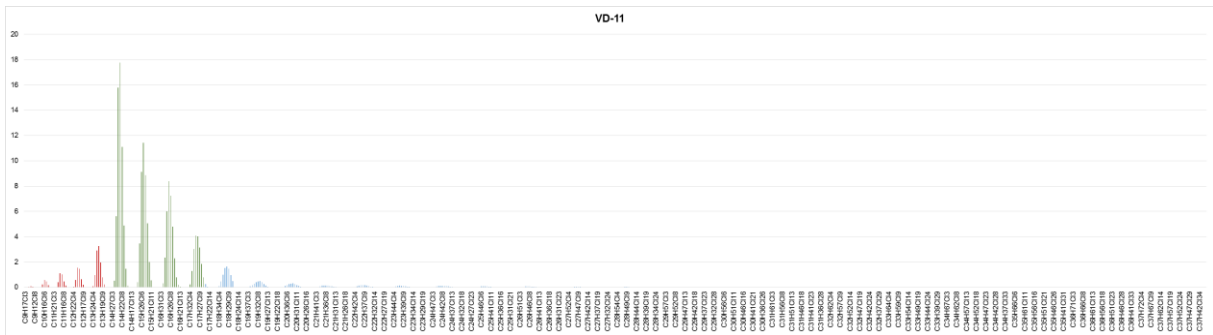


Fig. S23. Congener group patterns of CPs for VD-11

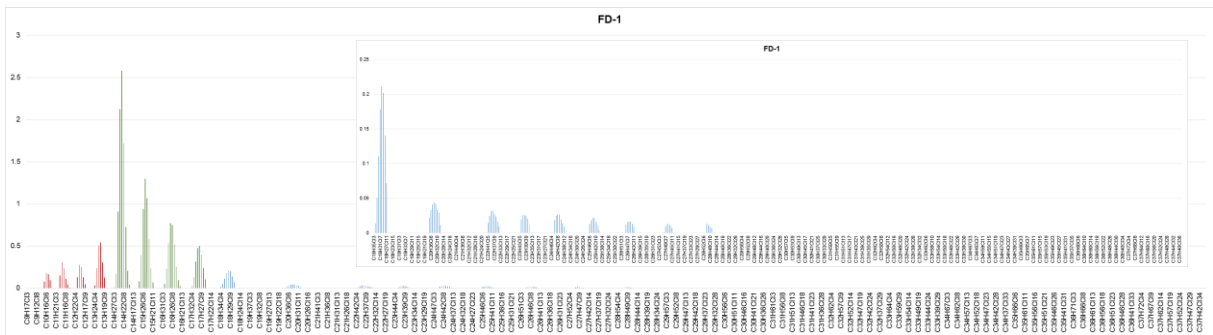


Fig. S24. Congener group patterns of CPs for FD-1, the enlarged region show the pattern for C₁₈ to C₃₁

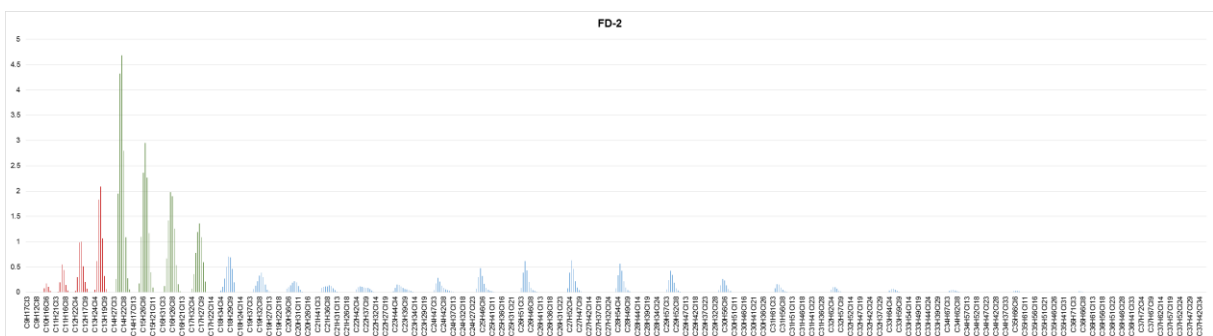


Fig. S25. Congener group patterns of CPs for FD-2

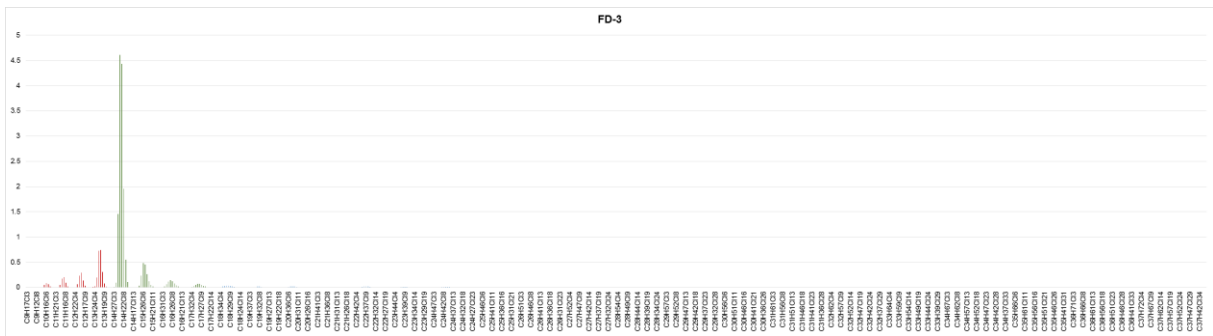


Fig. S26. Congener group patterns of CPs for FD-3

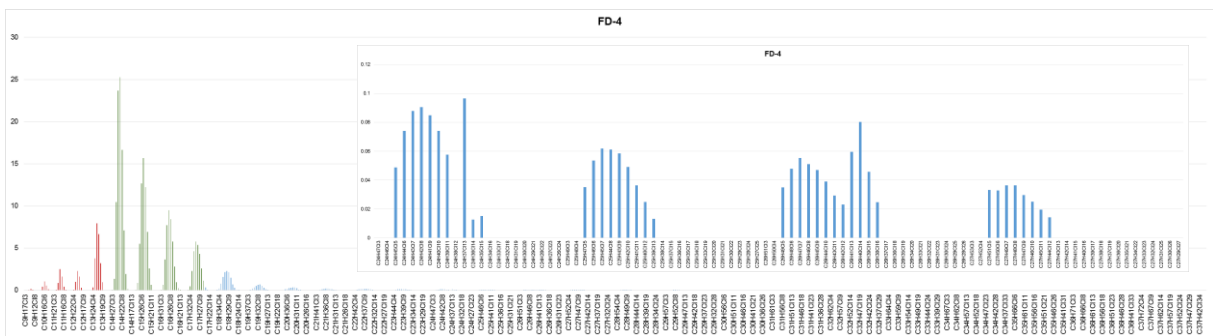


Fig. S27. Congener group patterns of CPs for FD-4, the enlarged region show the double chlorination peak observed for C₂₄ to C₂₇

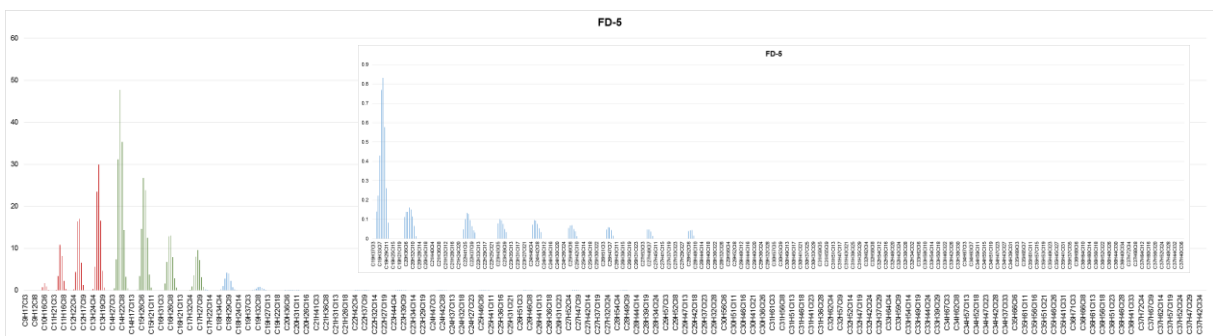


Fig. S28. Congener group patterns of CPs for FD-5, the enlarged region show the pattern for C₁₉ to C₃₇

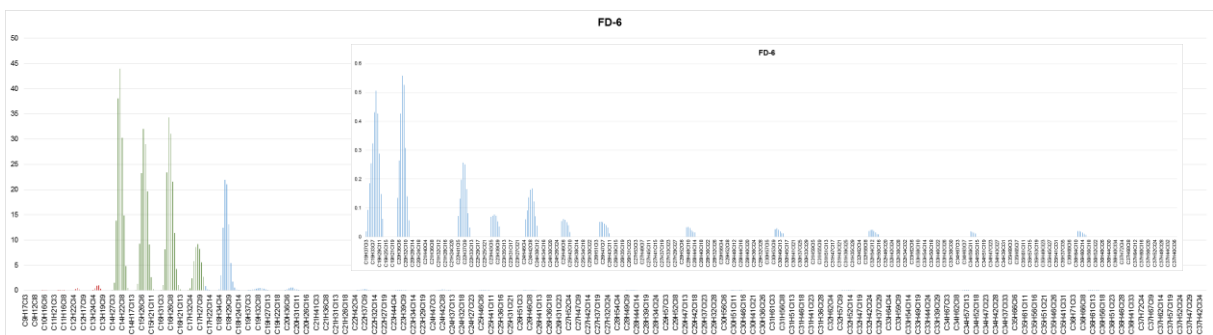


Fig. S29. Congener group patterns of CPs for FD-6, the enlarged region show the CP pattern from C₁₉ to C₃₇, no C₂₁ was observed and from C₂₆ only even carbon chain lengths were observed.

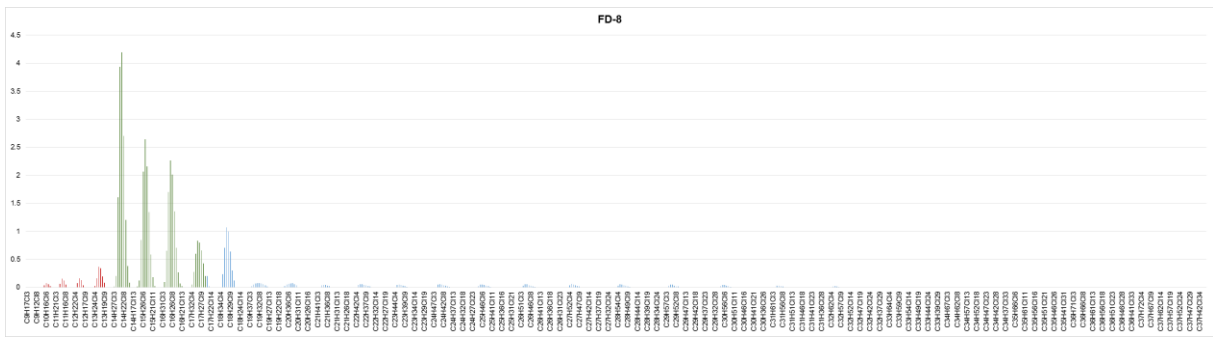


Fig. S30. Congener group patterns of CPs for FD-8

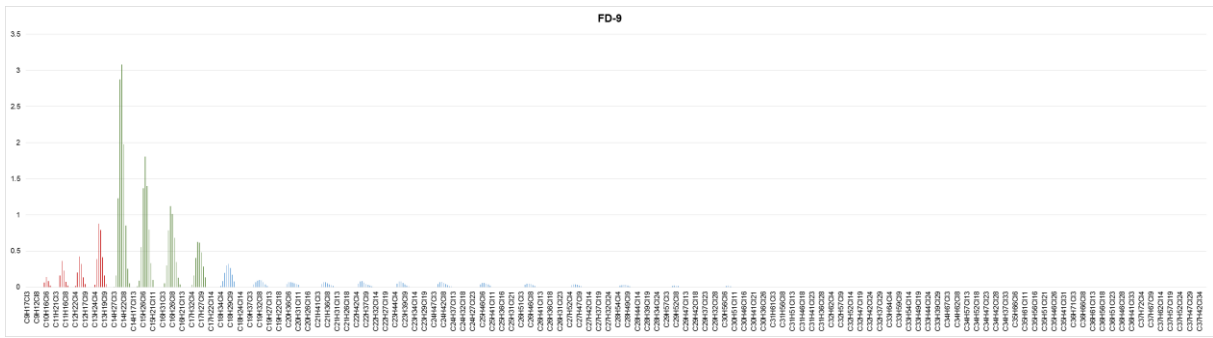


Fig. S31. Congener group patterns of CPs for FD-9

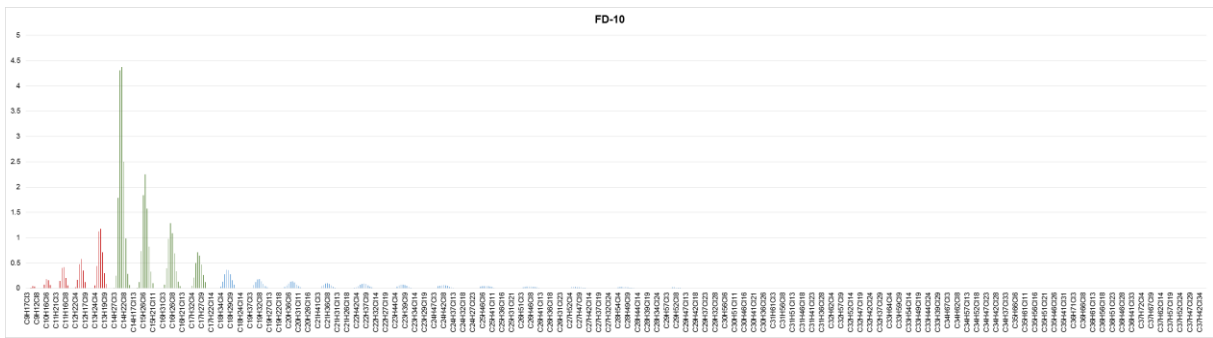


Fig. S32. Congener group patterns of CPs for FD-10

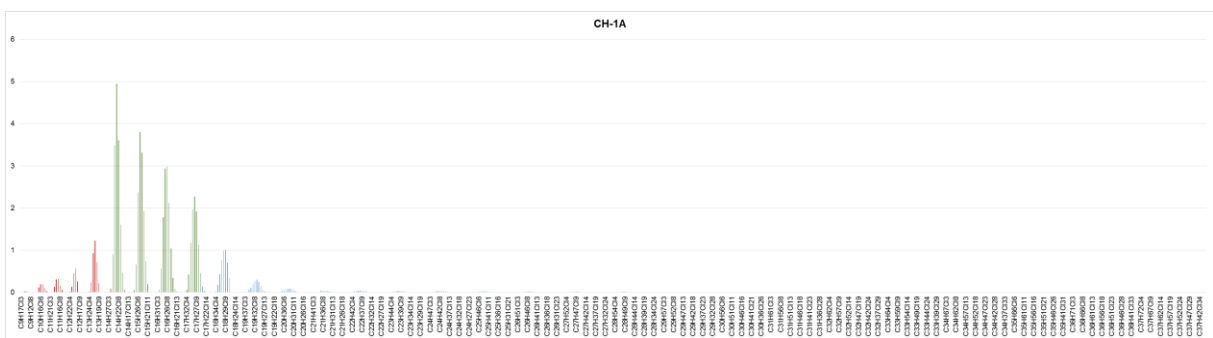


Fig. S33. Congener group patterns of CPs for CH-1A

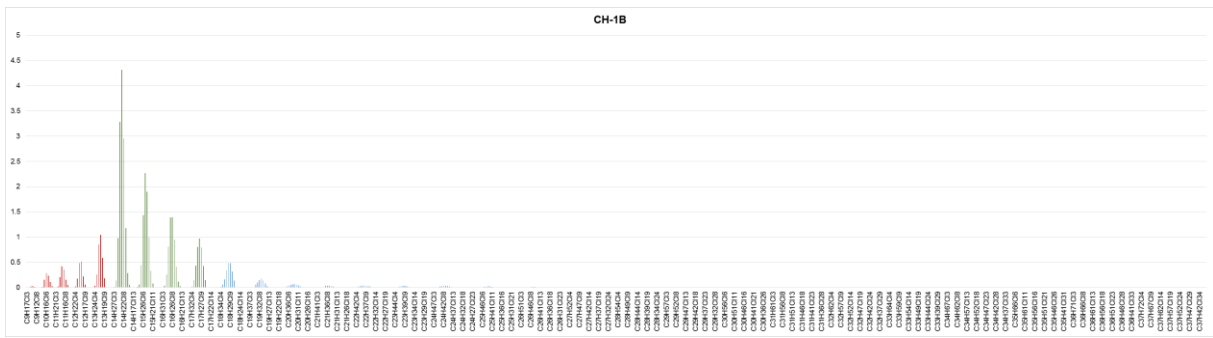


Fig. S34. Congener group patterns of CPs for CH-1B

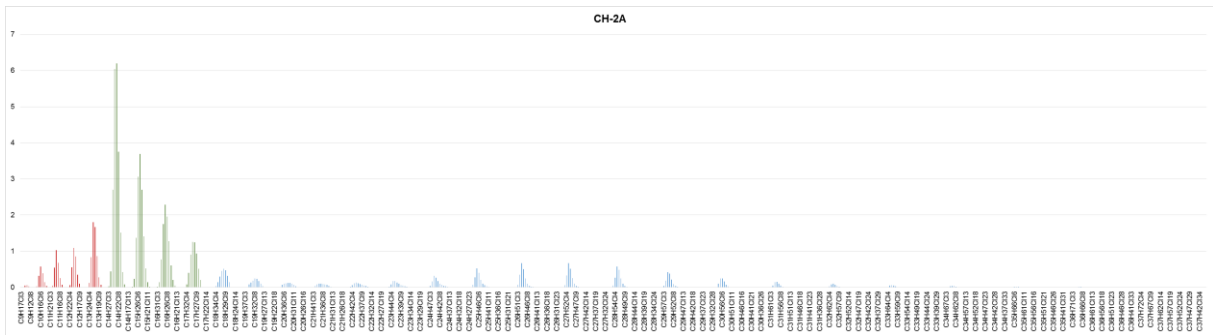


Fig. S35. Congener group patterns of CPs for CH-2A

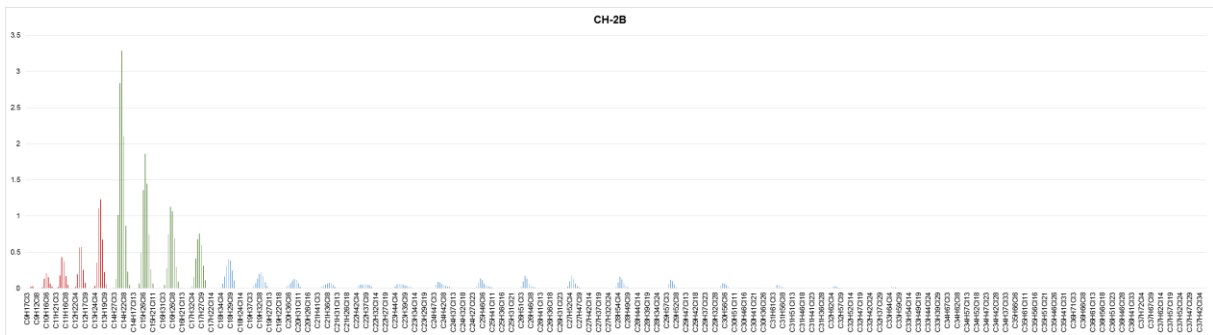


Fig. S36. Congener group patterns of CPs for CH-2B

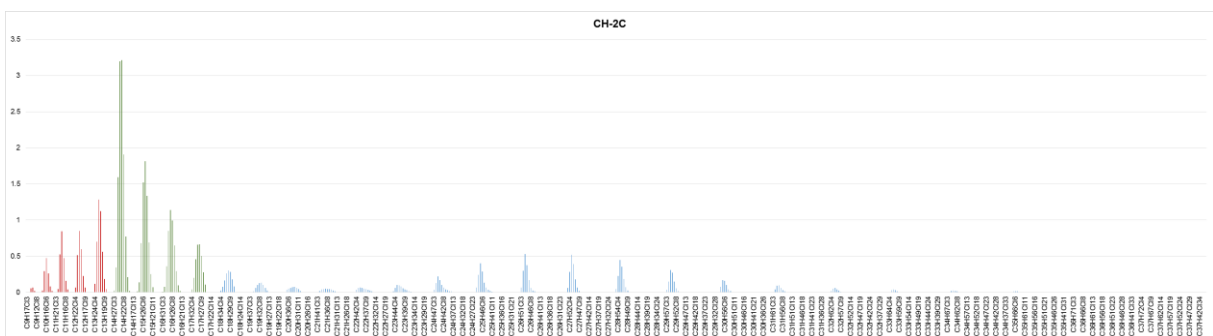


Fig. S37. Congener group patterns of CPs for CH-2C

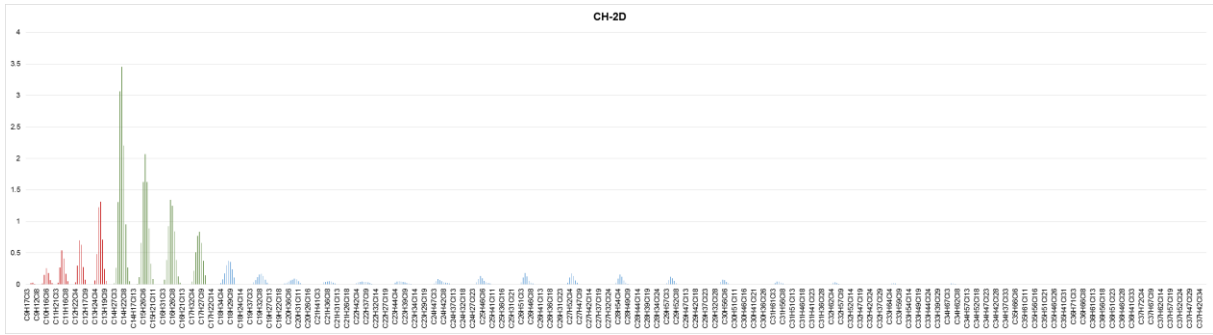


Fig. S38. Congener group patterns of CPs for CH-2D

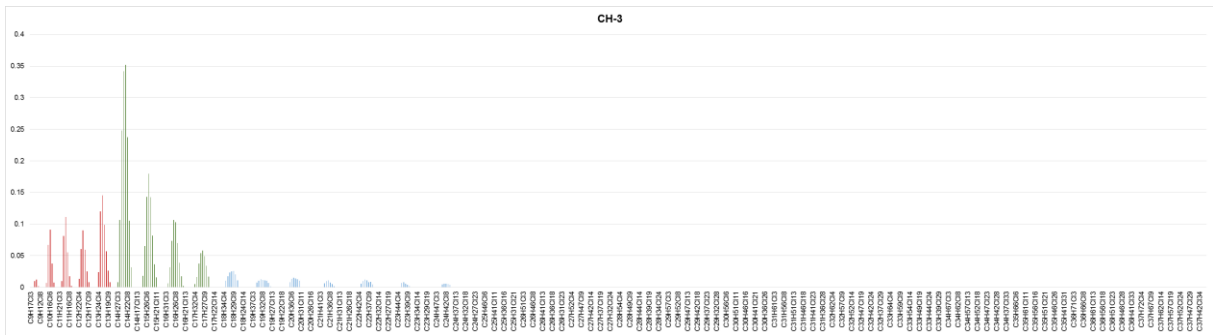


Fig. S39. Congener group patterns of CPs for CH-3

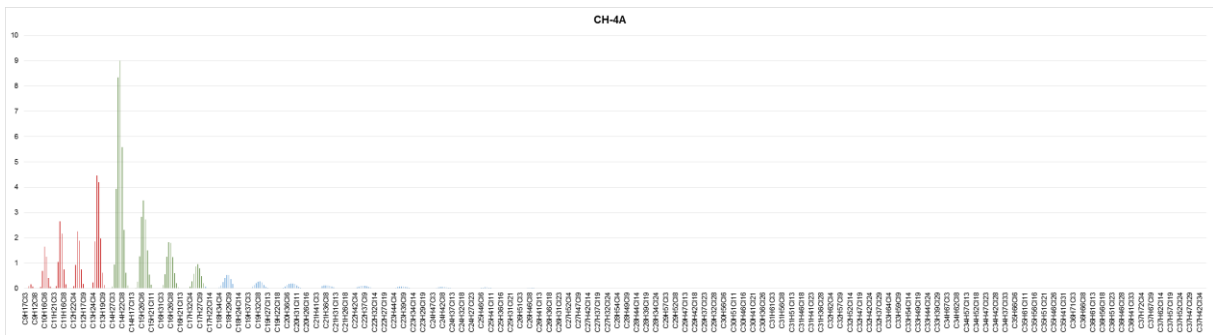


Fig. S40. Congener group patterns of CPs for CH-4A

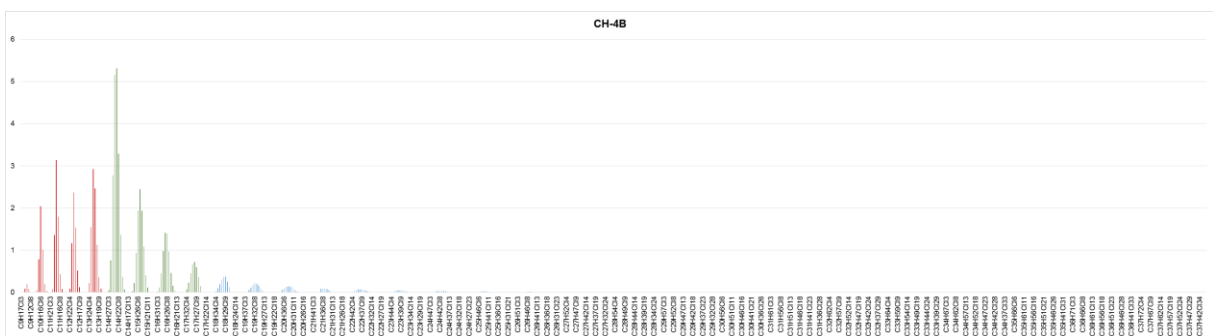


Fig. S41. Congener group patterns of CPs for CH-4B

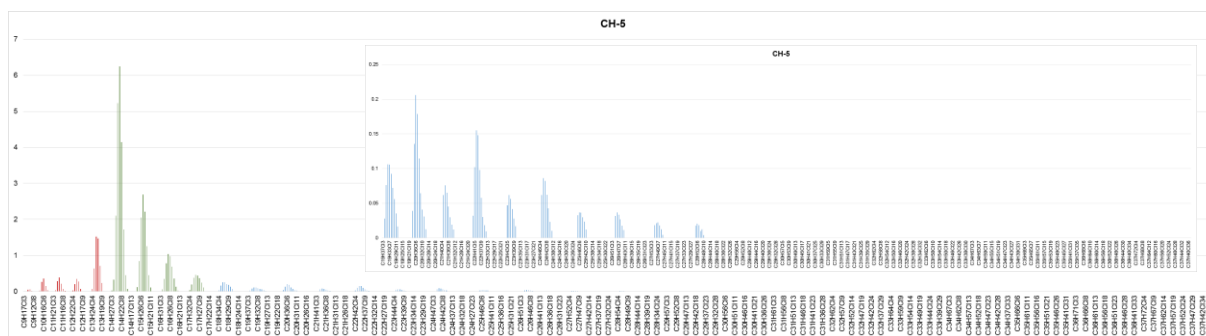


Fig. S42. Congener group patterns of CPs for CH-5, the enlarged region show the pattern for C₁₉ to C₃₇

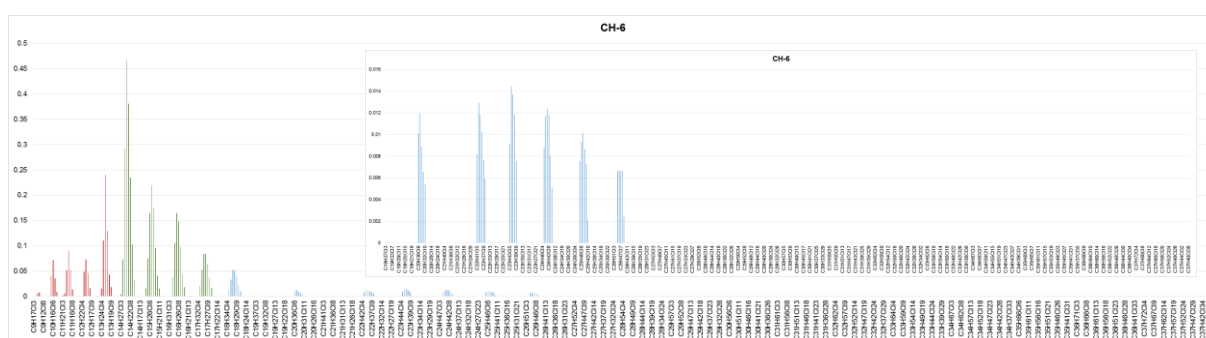


Fig. S43. Congener group patterns of CPs for CH-6, the enlarged region show the pattern for C₁₉ to C₃₇

REFERENCES

- Chen, H., Lam, J.C.W., Zhu, M., Wang, F., Zhou, W., Du, B., Zeng, L., Zeng, E.Y., 2018. Combined Effects of Dust and Dietary Exposure of Occupational Workers and Local Residents to Short- and Medium-Chain Chlorinated Paraffins in a Mega E-Waste Recycling Industrial Park in South China. *Environ. Sci. Technol.* 52, 11510–11519. doi:10.1021/acs.est.8b02625
- Chen, Y.H., Chang, C.Y., Ding, W.H., 2016. Vortex-homogenized matrix solid-phase dispersion for the extraction of short chain chlorinated paraffins from indoor dust samples. *J. Chromatogr. A* 1472, 129–133. doi:10.1016/j.chroma.2016.10.048
- Fridén, U.E., Mclachlan, M.S., Berger, U., 2011. Chlorinated paraffins in indoor air and dust: Concentrations, congener patterns, and human exposure. *Environ. Int.* 37, 1169–1174. doi:10.1016/j.envint.2011.04.002
- Gao, W., Cao, D., Wang, Yingjun, Wu, J., Wang, Ying, Wang, Yawei, Jiang, G., 2018. External Exposure to Short- and Medium-Chain Chlorinated Paraffins for the General Population in Beijing, China. *Environ. Sci. Technol.* 52, 32–39. doi:10.1021/acs.est.7b04657
- He, C., Brandsma, S.H., Jiang, H., O'Brien, J.W., van Mourik, L.M., Banks, A.P., Wang, X., Thai, P.K., Mueller, J.F., 2019. Chlorinated paraffins in indoor dust from Australia: Levels, congener patterns and preliminary assessment of human exposure. *Sci. Total Environ.* 682, 318–323. doi:10.1016/j.scitotenv.2019.05.170
- Hilger, B., Fromme, H., Völkel, W., Coelhan, M., 2013. Occurrence of chlorinated paraffins in house dust samples from Bavaria, Germany. *Environ. Pollut.* 175, 16–21.

doi:10.1016/j.envpol.2012.12.011

- Huang, X., Liu, Q., Gao, W., Wang, Y., Nie, Z., Yao, S., Jiang, G., 2018. Fast screening of short-chain chlorinated paraffins in indoor dust samples by graphene-assisted laser desorption/ionization mass spectrometry. *Talanta* 179, 575–582. doi:10.1016/j.talanta.2017.11.055
- Liu, L.H., Ma, W.L., Liu, L.Y., Huo, C.Y., Li, W.L., Gao, C.J., Li, H.L., Li, Y.F., Chan, H.M., 2017. Occurrence, sources and human exposure assessment of SCCPs in indoor dust of northeast China. *Environ. Pollut.* 225, 232–243. doi:10.1016/j.envpol.2017.03.008
- Shang, H., Fan, X., Kubwabo, C., Rasmussen, P., 2019. Short-chain and medium-chain chlorinated paraffins in Canadian house dust and NIST SRM 2585. *Environ. Sci. Pollut. Res.* doi:10.1007/s11356-018-04073-2
- Shi, L., Gao, Y., Zhang, H., Geng, N., Xu, J., Zhan, F., Ni, Y., Hou, X., Chen, J., 2017. Concentrations of short- and medium-chain chlorinated paraffins in indoor dusts from malls in China: Implications for human exposure. *Chemosphere* 172, 103–110. doi:10.1016/j.chemosphere.2016.12.150
- Wong, F., Suzuki, G., Michinaka, C., Yuan, B., Takigami, H., de Wit, C.A., 2017. Dioxin-like activities, halogenated flame retardants, organophosphate esters and chlorinated paraffins in dust from Australia, the United Kingdom, Canada, Sweden and China. *Chemosphere* 168, 1248–1256. doi:10.1016/j.chemosphere.2016.10.074